EUROFUSION WP14ER-PR(16) 15882

BW Shanahan et al.

Simulating blob dynamics in TORPEX null point configurations using BOUT++

Preprint of Paper to be submitted for publication in
Plasma Physics and Controlled Fusion

This work has been carried out within the framework of the EUROfusion Consortium and has received funding from the Euratom research and training programme 2014-2018 under grant agreement No 633053. The views and opinions expressed herein do not necessarily reflect those of the European Commission.

Simulating blob dynamics in TORPEX null point configurations using BOUT++

B W Shanahan and B D Dudson

York Plasma Institute, Department of Physics,

University of York, Heslington, York YO10 5DD, UK[*]

Abstract

Three dimensional blob dynamics are simulated in X-point magnetic configurations in the TORPEX device via a non-field-aligned coordinate system, using an isothermal model which evolves density, vorticity, parallel velocity and parallel current density. By modifying the parallel gradient operator to include perpendicular perturbations from poloidal field coils, numerical singularities associated with field aligned coordinates are avoided. Blobs are found to propagate according to the sheath-connected scaling, and a validation with experiment is performed. It is determined that the null region can cause an acceleration of filaments due to increasing connection length, but this accleration is small relative to other effects, which we quantify. A comparison with a previously developed analytical model [1] is performed and an agreement is found with minimal modification. Experimental measurements [1] are reproduced, and the dominant acceleration mechanism is identified as that of a developing dipole in a moving background. Contributions from increasing connection length close to the null point are a small correction.

[*] bws502@york.ac.uk

I. INTRODUCTION

Filaments, or blobs, are field aligned plasma structures which have been observed in the scrape of layer (SOL) of many magnetically confined plasmas [2]. These filaments carry particles into the SOL and therefore play a role in determining the profiles during L-mode and inter-ELM H-mode scenarios. While there have been many investigations into the dynamics of such filaments [2–4], few if any have studied their behavior near magnetic X-points. Simple magnetic tori such as the TORPEX device [5] replicate tokamak scrape off layer (SOL) scenarios while allowing straightforward diagnostic access. While filaments have been studied extensively experimentally within TORPEX [6–8], no theoretical studies have yet explored the dynamics in X-point configurations recently studied experimentally [9].

The fundamental physics of blob propagation is described in detail in [2] which is as follows. Diamagnetic drifts polarize the blob, leading to an $\mathbf{E} \times \mathbf{B}$ velocity in the form of counter-rotating vortices and an outward advection of the blob. The dynamics of propagating filaments depends on the mechanism for charge dissipation within the blob in order to satisfy quasineutrality, $\nabla \cdot j = 0$. If the charge separation caused by diamagnetic drifts is resolved primarily via the parallel current through the sheath, the filament is considered to be sheath-connected. If the connection length to the sheath is too large, or likewise the resistivity too large, charge is dissipated via the polarization current and the blob is said to be in the inertially limited regime.

In this work filaments are characterized in TORPEX magnetic null point scenarios using three dimensional simulations in `BOUT++` [10]. The research presented here focuses on the behavior of filaments as they encounter both open and closed field lines, and how that simulated behavior relates to experimentally observed characteristics.

A. TORPEX null point scenarios

The aim of this work is to explore blob dynamics in the TORPEX simple magentic torus in X-point geometries [9]. The magnetic geometry which was simulated is shown in Figure 1, along with the density contour of a seeded blob.

The TORPEX device has a major radius of 1m, minor radius of 20cm, and a toroidal magnetic field of about 75mT [9]. The implementation of the complex poloidal magnetic

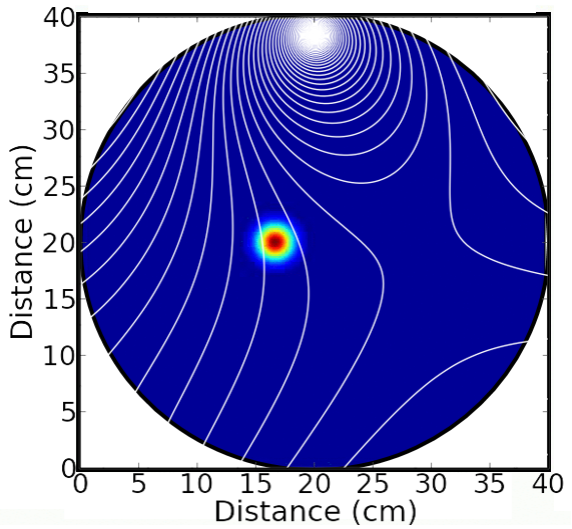

FIG. 1. Poloidal cross section indicating the magnetic geometry of TORPEX X-point scenarios (white contours) and the gaussian seeded blob (color contour).

field is discussed in Section II B.

II. NUMERICAL METHODS AND MODEL

A. Isothermal Model

An isothermal cold-ion fluid model initially constructed for plasma blob studies [3, 11] has been extended for use in X-point scenarios [12]. The model is electrostatic and inviscid; the isothermal electron temperature T_{e0} is set to 2.5eV [13]. While this model includes several simplifications, it still captures relevant physics such as Kelvin-Helmholtz, interchange and driftwave turbulence, an important class of instabilities in tokamak edge plasmas [14] as it is a ubiquitous instability. The equations which are solved are given as follows in SI units:

$$\frac{dn}{dt} = (1-\chi)\left[2c_s\rho_s\xi\cdot(\nabla n - n_0\nabla\phi) + \nabla_\parallel\frac{J_\parallel}{e} - n_0\nabla_\parallel u_\parallel\right] + \chi\nabla_\parallel^2 n \tag{1}$$

$$\rho_s^2 n_0\frac{d\Omega}{dt} = 2c_s\rho_s\xi\cdot\nabla n + \nabla_\parallel\frac{J_\parallel}{e} - \zeta\Omega \tag{2}$$

$$\frac{du_\parallel}{dt} = -\frac{c_s^2}{n_0}\nabla_\parallel n \tag{3}$$

$$J_\parallel = (1-\chi)\left[\frac{\sigma_\parallel T_e}{en_0}(\nabla_\parallel n - n_0\nabla_\parallel\phi)\right] \tag{4}$$

Where $\Omega \equiv \nabla_\perp^2 \phi$ is the vorticity, total derivatives are split via $\frac{d}{dt} = \frac{\partial}{\partial t} + \mathbf{u_E} \cdot \nabla + \mathbf{u}_\parallel \cdot \nabla$, and parallel derivatives are evaluated using $\nabla_\parallel = \mathbf{b} \cdot \nabla$ where $\mathbf{b}$ is the unit vector along the total magnetic field, including the poloidal field. Curvature effects are included via the polarization vector $\xi \equiv \nabla \times \frac{\mathbf{b}}{B} \sim \frac{1}{R_c}\hat{\mathbf{z}}$. In the above equations, $\rho_s = \frac{c_s}{\Omega_i}$ is the Bohm gyroradius. These equations are normalized such that density (n) is normalized to typical TORPEX values, $n_0 = 5 \times 10^{16} m^{-3}$, speeds are normalized to the sound speed, and $\phi = \frac{e\Phi}{T_{e0}}$ is the normalized electrostatic plasma potential.

Because TORPEX utilizes an in-vessel coil to create the X-point field, the singularity on the coil axis (described in the following section) has been avoided by implementing a penalization scheme [15], which utilizes a masking function at the location of the wire such that there are no gradients across the coil cross section. The masking function (χ) has the following form:

$$\chi = \begin{cases} 1 & 0 < r < r_c \\ \chi_0 \, ln(r) & r_c \leq r \leq 1.1 r_c \\ 0 & r > 1.1 r_c \end{cases}$$

Where r_c is the coil radius, chosen here to be 1cm, and χ_0 is an arbitrary coefficient to determine the smoothness of the masking function. The final term in Equation 2 serves as a simplified model for neutral collisions. It has been shown that collisions can slow blob propagation in TORPEX [8]. Here, our ion-neutral collision is considered to be charge exchange and is of the form $\zeta = 2 \times 10^{-14} n_n / \Omega_{ci}$, where n_n is the density of neutrals in the system [16].

This model differs from that used in reference [3] in that it incorporates parallel ion free streaming, $u_\parallel$, as parallel flows are vital when determining the effects of X-points. Additionally, energy conservation required the restriction that n is considered constant (n_0) in terms where it is not differentiated such as the right hand side of Equation 3, which is simply a limit of the imposed Boussinesq approximation which assumes that density fluctuations are small: $\nabla \times \left(n \frac{d \nabla_\perp \phi}{dt} \right) \approx n_0 \frac{d}{dt} \nabla_\perp^2 \phi$.

B. Numerical Methods

The presence of poloidal magnetic field singularities in the form of O- and X-points in this magnetic topology requires the use of non-field-aligned coordinate systems. As such, a cylindrical coordinate system defined by the major radius ($\mathbf{x}$), vertical direction($\mathbf{z}$), and toroidal direction ($\mathbf{y}$) was implemented, and the poloidal magnetic field implemented by prescribing an analytic form for the magnetic vector potential and modifying the parallel gradient operator [17]:

$$\mathbf{A}(\mathbf{r}) = \frac{-\mu_0 I}{2\pi} \ln(r)\hat{\mathbf{y}} \tag{5}$$

where $\hat{\mathbf{y}}$ is the toroidal direction (parrallel to wire). It is therefore possible to construct an arbitrary magnetic field given the number of turns, current, and location of magnetic coils. The only difficulty is the infinite magnetic field on axis, which is avoided using a penalization scheme, as described in the previous section. Our form of the vector potential can therefore be implemented into our simulationsm as the $\mathbf{b} \cdot \nabla$ operator such that:

$$\mathbf{b} \cdot \nabla f = \nabla_{\parallel} f - \left[\frac{A_{ext}}{B}, f\right] \tag{6}$$

where A_{ext} is the perturbed externally applied vector potential due to the magnetic coils and the square brackets are Poisson brackets which are solved using the Arakawa method [18].

The model described in Section II A is solved in this geometry using a resolution of 1.15mm ($1.25\rho_s$) in the plane perpendicular to $\mathbf{B}$ ($\mathbf{x}$, $\mathbf{z}$), and 8cm ($90.4\rho_s$) in direction parallel to $\mathbf{B}$ ($\mathbf{y}$). Time integration was implemented using the implicit time integration solver CVODE, within the SUite of Nonlinear abd DIfferential/ALgebraic equation Solvers (SUNDIALS) [19]. Finally, the Laplacian solver, which calculates potential (ϕ) from vorticity (Ω), in `BOUT++` was altered to invert using discrete sine transforms in the $\mathbf{z}$ direction (perpendicular to $\mathbf{B}$ in the azimuthal plane), which eliminates the periodicity used in typical Laplacian inversion utilizing Fourier transforms in `BOUT++` [10].

III. FILAMENT CHARACTERIZATION AND EXPERIMENTAL COMPARISON

Simulations were performed to validate the extension to toroidal geometries of the model described previously and to determine the characteristics of blob propagation within the TORPEX magnetic null point scenarios. Experimental comparison was conducted to investigate the filament acceleration mechanism seen in experiment. It has been proposed elsewhere that the poloidal magnetic null region causes an acceleration by increasing the connection length associated with the dipole field [1].

A. Filament characterization

As described in Section I, filaments are often characterized by the mechanism for charge dissipation within the system. If the dipole is predominently disspiated by parallel currents, the filament is considered to be sheath limited. Alternatively, if the potential dipole is short circuited by the polarization current, it is considered to be inertially limited. Plotting blob velocity as a function of the initial size of the filament illustrates the various propagation regimes, as filament regimes are dependent on the perpendicular size of the filament [8, 20, 21], as shown in Figure 2. Additionally, we can plot the relative contributions of the parallel and polarization current to determine the regime of propagation. This is shown in Figure 3.

Figure 2 indicates that the blobs are within the sheath-limited regime, as the filaments follow a scaling of δ^{-2}, where δ is the size of the filament. The filaments observed in TORPEX are between 2cm and 4cm in diameter [1], which is confirmed by this scaling as this size is the transition between the sheath and inertially limited regimes – where filaments are the most stable [22].

Likewise, Figure 3 supports the hypothesis that these filaments are intially in the sheath-limited regime, as the parallel current dominates over the polarization current. Previous analysis [8, 21] has also indicated that filaments in TORPEX hydrogen plasmas are sheath connected, however those simulations were performed in the typical vertical field configuration and did not include the magnetic null as modelled here.

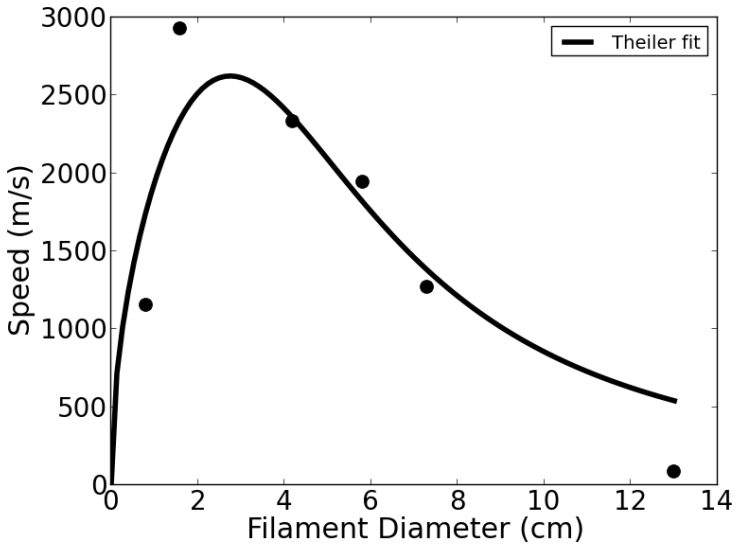

FIG. 2. Parameter scan of the blob velocity as a function of filament diameter, and the fitted relation according to [8].

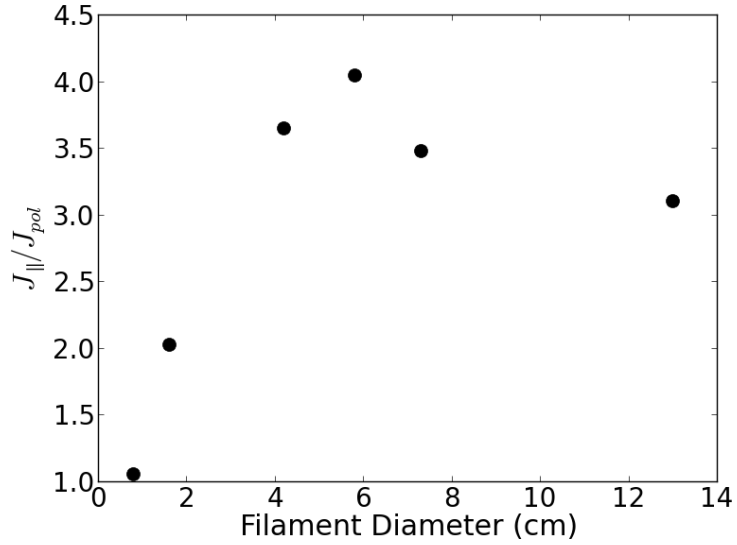

FIG. 3. Ratio of the maximum parallel current to the maximum polarization current as a function of filament diameter, indicating that all scenarios occur in the sheath-limited regime, as parallel currents are dominant.

B. Stationary Background

Having characterized the regimes of filament propagation, an attempt to validate simulation methods with experimental measurements of blob velocity was conducted. Initial

simulations were performed with a stationary background plasma profile. To compare with experiment, the center of mass velocity was calculated and plotted for comparison with experimental data [1]. The results of this analysis are summarized in Figure 8, where the simulations in a stationary background are plotted as a solid line. These simulations can be compared to the background subtracted velocity profile in Figure 3 in the recent paper by Avino *et al* [1], and are shown later in Figure 8 in Section III D.

From this data, it is clear that although the simulations match the velocity of the blob propagation, they do not exhibit the same acceleration seen in experiment. The acceleration found in experiment is much higher than that of the simulations in the region of the X-point. However, it is still possible to determine the effect of the magnetic null region on filament propagation by seeding blobs at various distances from the magnetic null and measuring their velocities as they approach the X-point. The results of these simulations are shown in Figure 4.

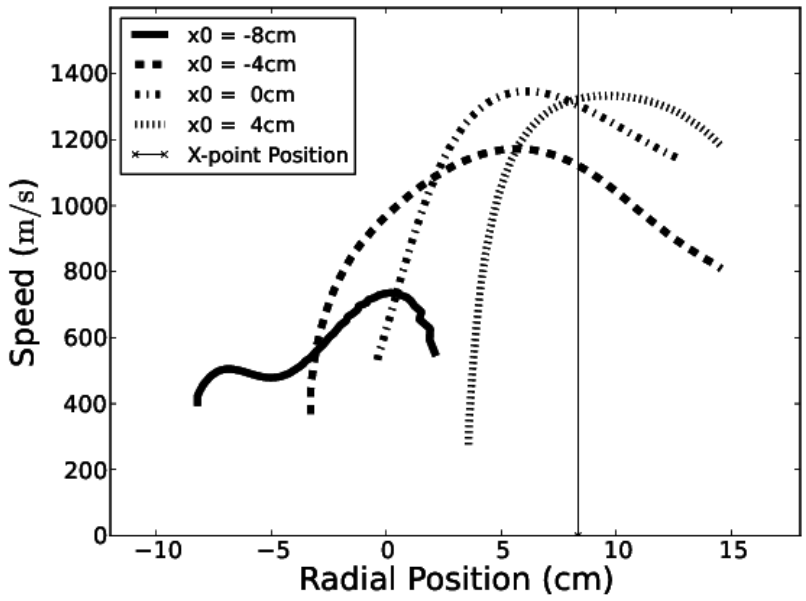

FIG. 4. Velocity comparison of blobs seeded at various distances from the X-point. Faster blob propagation is seen near the null region.

The acceleration of the various seeded blobs is illustrated in Figure 4. Filaments have a higher acceleration at the beginning of their evolution due to the developing dipole, and continue to accelerate more slowly as they approach the X-point. This supports the assertion that the magnetic null point region causes an acceleration of filaments, most likely due to

the increased connection length. However, as the strongest acceleration occurs during the formation of the dipole (e.g. $\sim 8 \times 10^7 \mathrm{ms}^{-2}$ for the case seeded at $x_0 = 4\mathrm{cm}$), these results could indicate that the acceleration seen in experiment is due to the dipole forming on a moving background (which is itself approaching the null region). This hypothesis will be further tested in Section III D.

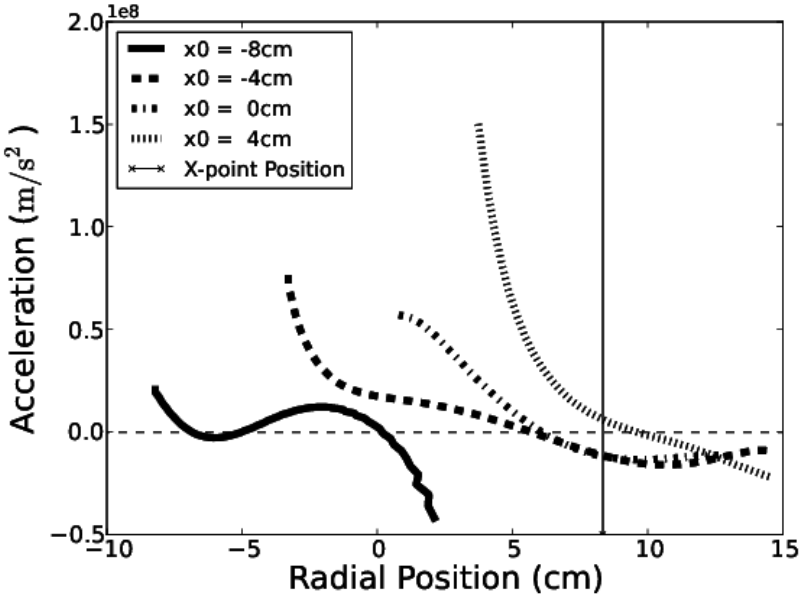

FIG. 5. Comparison of acceleration of blobs seeded at various distances from the X-point. The highest acceleration occurs initially, as a dipole is developing.

To determine if the effects modelled here are consistent with previous analysis of TORPEX X-point scenarios [1, 13], a comparison with an analytic model [1, 13] of blob propagation in magnetic null regions was performed.

C. Analytical model comparison

An analytical model has been previously developed which relies on the assumption of increasing connection length in poloidal magnetic null regions as an acceleration mechanism [1, 13]. As a result the blob velocity follows a function as shown in Equation 7:

$$v_b = \frac{\delta n}{n} \sqrt{\frac{2a}{R}} c_s \left(\frac{1}{1 + A/L_\parallel} \right) \tag{7}$$

where:

$$A = \frac{CB^2 a^{5/2}\sqrt{2R}}{m_i c_s} \tag{8}$$

Here, C is the proportionality coefficient between the plasma conductivity and the plasma density ($C = \sigma/n$), a is the is the diameter of the blob, $L_\parallel$ is the parallel connection length, R is the major radius, and c_s is the sound speed. In the original analysis, the relative perturbation of density, $\delta n/n$, was considered constant, and therefore the magnetic field (B), which also dictates the parallel connection length $L_\parallel$, is considered the only position-dependent variable. In the analysis presented here, however, we are able to directly calculate all quantities in Equation 7 from numerical simualtions.

The only quantity used in this model which is not directly available from simulations is the plasma conductivity as calculated in Reference [1]:

$$\sigma = \frac{ne}{m_e \nu_{eH}} \tag{9}$$

where $\nu_{eH} = n_n \sigma_{eH}\sqrt{T_e/m_e}$ is the electron-neutral collision frequency. In these simulations, we have assumed the neutral density n_n is $2 \times 10^{18}\mathrm{m}^{-3}$ and a collisional cross section $\sigma_{eH} = 2 \times 10^{-19}\mathrm{m}^2$ following the analysis of [23]. As stated previously, an isothermal temperature of 2eV was assumed.

The blob size a can be calculated as the distance between the maximum and minimum of the potential dipole. Connection length is calculated by assuming that:

$$L_\parallel = \frac{a}{tan\left(\frac{\delta B}{B}\right)} \tag{10}$$

where $\delta B/B$ is the poloidal magnetic field over the toroidal magnetic field. In completely vertical field cases, this reduces to B_z/B.

This model was then plotted against the stationary background simulation shown in Figure 8 along with the calculations from Reference [1]. The proportionality coefficient C is adjusted such that the calculated blob velocity coincides with our simulation 28μs prior to the filament arriving at the X-point. This is also done in Reference [1], where the proportionality constant is three times that calculated analytically. Here, the proportionality constant is decreased by a factor of 1.8 ($C = 0.56C_{analytic}$) relative to the analytic solution, whereas C was increased by a factor of 3 in [1]. Figure 6 illustrates the simulation, previous analytical

results, and the calculations based on the simulation presented here with and without an adjustment to the proportionality constant.

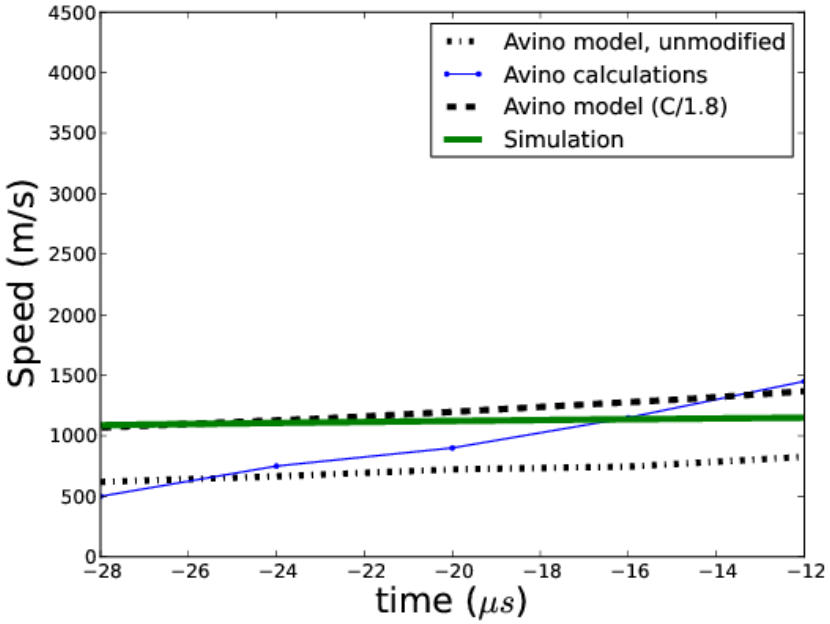

FIG. 6. Comparison of simulated blob velocities (on a stationary background) with an analytical model [1]. Simulated results are shown in green, whereas original calculations from [1] are in blue. The model explicitly calculated herein is shown in black, dashed, both with and without an adjustment to the proportionality coefficient. Here, as with [1], t=0 is when the blob is at the null point.

From Figure 6 it is not clear how well the analytical model expressed in Equation 7 reproduces the data. Explicitly calculating the values used in simulation does however support the observation that the accleration seen in experiment is not primarily caused by the increasing connection length as this model describes, as the analytical model (black, dashed) exhibits a lower acceleration than that seen in experiment, as shown by the original data from [1] in blue. Therefore, Figure 6 implies that the accleration seen in experiment is not only due to the increasing connection length in the mangetic null region.

The same analysis was conducted on a filament seeded farther from the magnetic null region. This allows the filament dipole to fully develop before encountering any effects of the X-point. The results are shown in Figure 7. This supports the hypothesis that the increasing connection length $L_{\|}$ in the region of the X-point causes an acceleration, as the model de-

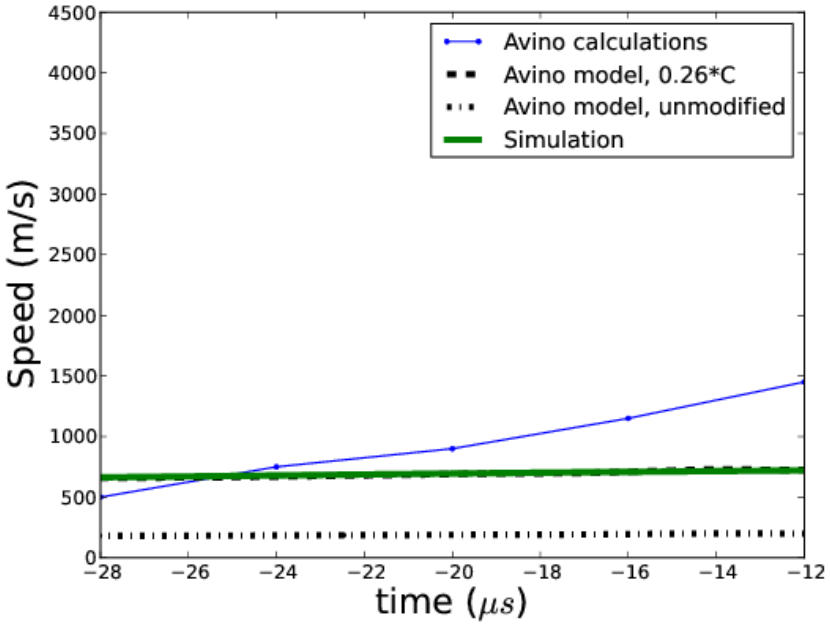

FIG. 7. Comparison of simulated blob velocities (on a stationary background) with an analytical model [1]. Here, the filaments are seeded farther from the X-point, at r_0 = -8cm to allow the dipole to fully develop. Simulated results are shown in green, whereas original calculations from [1] are in blue. The model explicitly calculated herein is shown in black, dashed, both with and without an adjustment to the proportionality coefficient.

scribed in Reference [1] reproduces results seen in simulations. Here, the proportionality coefficient C was decreased by a factor of 3.8 relative to the analytic solution($C = 0.26C_{analytic}$). As the analytical model exhibits the same acceleration profile as shown in simulation, it is plausible to conclude that the accleration seen in the simulations is due to the introduction of the X-point. This acceleration, however, is smaller than that seen in experiment. We now show that the accleration seen in experiment is characteristic of the initial dipole formation. If the developing dipole were advected toward the X-point, it could appear that the magnetic null region is causing the accleration, when in actuality the effect of the null region on the accleration is minimal (as shown here). To test the assertion of an advected dipole creating the accleration profile seen in experiment, a moving background was added to the simulations, corresponding to a vertical electric field observed in experiments which created the background velocity measured in [1].

D. Constant translational background

To investigate if the initial dipole development causes the acceleration seen in experiment, a constant background radial plasma velocity of 2km/s was implemented in accordance with experimental measurements [1]. This was incorporated by implementing a background plasma potential profile with a constant gradient in **z**, thereby creating a constant radial $E \times B$ motion of the plasma. Figure 8 shows the results of three simulations. Simulations of blobs on a stationary background plasma profile, as discussed previously, is shown as the solid line. The dashed line indicates the velocity of blobs in a TORPEX X-point geometry with a moving background. When this is compared with the experimental measurements in Reference [1], it is clear that the simulation has more closely reproduced the experimentally observed acceleration and deceleration.

Not only does this case match the velocity seen in experiment, but the average acceleration and deceleration is reproduced. There is a slight difference in the maximum velocity which could potentially be attributed to the isothermal and inviscid approximations.

To verify that this effect is an effect of dipole formation and not the null region increasing connection length, we can overplot the velocity in a vertical magnetic field case, where no magnetic X-point is present. The results of this test case are also shown in Figure 8, where the dotted line indicates the blob propagation in a vertical field case with a moving background.

Figure 8 indicates that filaments in a vertical field have similar acceleration and velocity characteristics to those in magnetic X-point scenarios. Additionally, the differences in velocity profiles seen in simulation lie within the experimental uncertainty [1]. From these results it is possible to conclude that the acceleration mechanism seen in experiment is not primarily due to the increased connection length in the region of the X-point. Instead, the moving background causes the developing dipole to propagate towards the null region as it begins to accelerate the filament relative to the background. It should be noted that the recent experiments in magnetic null point geometries are not the first to exhibit the shown acceleration and deceleration profile. This characteristic has been seen previously in TORPEX vertical field scenarios both with simulation [24] and experiment [25]. It might be possible to measure the acceleration due to the X-point if the filament dipoles were allowed sufficient time to develop before entering the magnetic null region.

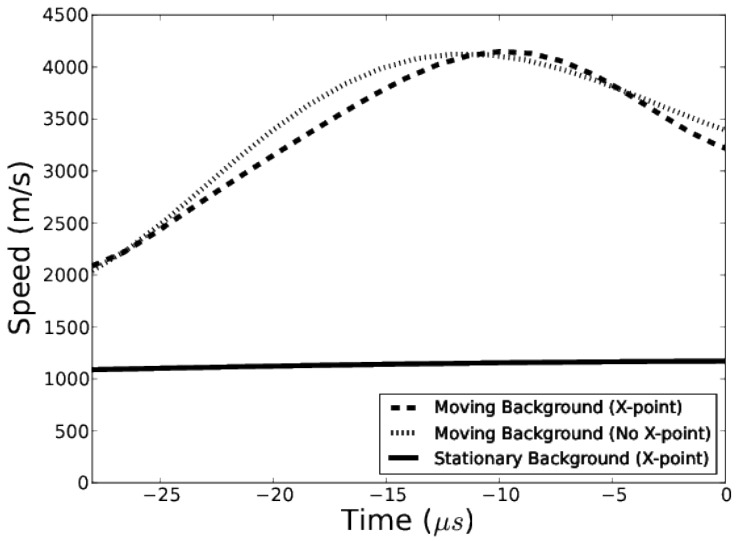

FIG. 8. Center of mass velocity measurements from simulations of three different scenarios; stationary background X-point case (solid), moving background X-point (dashed) and vertical (dotted) fields. The vertical field case in a moving background recovers the same characteristics as the X-point simulation and experimental measurements, indicating that the null region has little measureable effect on filament acceleration. This assertion is also supported by the small acceleration seen in the stationary background case (solid).

IV. CONCLUSIONS AND FUTURE WORK

We have successfully been able to model blob propagation in the X-point scenarios within the TORPEX device using a method of perturbed magnetic vector potentials. Experimental measurements could be reproduced, however simulation results indicate that the filament acceleration seen in experiment is due to dipole formation, and not the increased connection length caused by to the introduction of an X-point. It has also been shown that the magnetic null region does indeed cause an acceleration of filaments in the vicinity of the X-point. This acceleration, however, is much smaller than that of the initial dipole formation, and therefore is difficult to measure experimentally. However, if the magnetic null were created farther from the region where the filaments are formed, it would in principle be possible to measure the acceleration due to the increased connection length in the X-point region, provided the blob dipoles were given sufficient time to form. Future computational analysis of TORPEX configurations should look to implement a more complicated model which does not make an

isothermal approximation and more accurately incorporates neutrals.

Acknowledgments

This work has been carried out within the framework of the EUROfusion Consortium and has received funding from the Euratom research and training programme 2014-2018 under grant agreement No 633053. The views and opinions expressed herein do not necessarily reflect those of the European Commission. The authors acknowledge access to the ARCHER computing service through the Plasma HEC Consortium EPSRC grant number EP/L000237/1.

---

[1] F. Avino, A. Fasoli, I. Furno, P. Ricci, and C. Theiler, Phys. Rev. Lett. **116**, 105001 (2016).

[2] D. A. D´ Ippolito, J. R. Myra, and S. J. Zweben, Physics of Plasmas **18**, 060501 (2011).

[3] N. R. Walkden, B. D. Dudson, and G. Fishpool, Plasma Physics and Controlled Fusion **55**, 105005 (2013).

[4] J. R. Myra, D. A. Russell, and D. A. DIppolito, Physics of Plasmas **13**, 112502 (2006), http://dx.doi.org/10.1063/1.2364858.

[5] A. F. et al., Plasma Physics and Controlled Fusion **52**, 124020 (2010).

[6] I. Furno, B. Labit, M. Podestà, A. Fasoli, S. H. Müller, F. M. Poli, P. Ricci, C. Theiler, S. Brunner, A. Diallo, and J. Graves, Phys. Rev. Lett. **100**, 055004 (2008).

[7] M. Podestà, A. Fasoli, B. Labit, I. Furno, P. Ricci, F. M. Poli, A. Diallo, S. H. Müller, and C. Theiler, Phys. Rev. Lett. **101**, 045001 (2008).

[8] C. Theiler, I. Furno, P. Ricci, A. Fasoli, B. Labit, S. H. Müller, and G. Plyushchev, Phys. Rev. Lett. **103**, 065001 (2009).

[9] F. Avino, A. Fasoli, and I. Furno, Review of Scientific Instruments **85**, 033506 (2014).

[10] B. D. Dudson, M. V. Umansky, X. Q. Xu, P. B. Snyder, and H. R. Wilson, Computer Physics Communications **180**, 1467 (2009).

[11] J. R. Angus, M. V. Umansky, and S. I. Krasheninnikov, Physical Review Letters **108**, 215002 (2012).

[12] B. W. Shanahan and B. D. Dudson, Journal of Physics: Conference Series **561**, 012015 (2014).

[13] F. Avino, *Turbulence at the boundary of toroidal plasmas with open and closed magnetic flux surfaces*, Ph.D. thesis, École Polytechnique Fédérale de Lausanne (EPFL), Centre de Recherches en Physique des Plasmas Association Euratom-Confédération Suisse.

[14] B. D. Scott, New Journal of Physics **4**, 52 (2002).

[15] L. Isoardi, G. Chiavassa, G. Ciraolo, P. Haldenwang, E. Serre, P. Ghendrih, Y. Sarazin, F. Schwander, and P. Tamain, Journal of Computational Physics **229**, 2220 (2010).

[16] P. C. Stangeby, *The Plasma Boundary of Magnetic Fusion Devices* (CRC Press, 2000).

[17] J. D. Jackson, *Classical Electrodynamics, Third edition* (John Wiley and Sons, 1999).

[18] A. Arakawa and V. R. Lamb, in *General Circulation Models of the Atmosphere*, Methods in Computational Physics: Advances in Research and Applications, Vol. 17, edited by J. Chang (Elsevier, 1977) pp. 173 – 265.

[19] "Advanced Computational Software collection, US DoE,".

[20] J. T. Omotani, F. Militello, L. Easy, and N. R. Walkden, Plasma Physics and Controlled Fusion **58**, 014030 (2016).

[21] L. Easy, F. Militello, J. Omotani, B. Dudson, E. Havlkov, P. Tamain, V. Naulin, and A. H. Nielsen, Physics of Plasmas **21**, 122515 (2014), http://dx.doi.org/10.1063/1.4904207.

[22] G. Q. Yu, S. I. Krasheninnikov, and P. N. Guzdar, Physics of Plasmas (1994-present) **13**, 042508 (2006).

[23] H. Tawara, Y. Itikawa, H. Nishimura, and M. Yoshino, Journal of Physical and Chemical Reference Data **19** (1990).

[24] F. D. Halpern, A. Cardellini, P. Ricci, S. Jolliet, J. Loizu, and A. Mosetto, Physics of Plasmas **21**, 022305 (2014).

[25] F. Riva and et al., Plasma Physics and Controlled Fusion **58**, 044005 (2016).